Computational Energy Science

Vol. 1, No. 4, p. 175-187, 2024

Original article

Numerical investigation of CO_2 solubility trapping mechanisms for enhanced storage in saline aquifers

Zeeshan Tariq[1]*, Jose Kevin Pauyac Estrada[1,2], Bicheng Yan[1]*, Jianchun Xu[3], Youwei He[4]

[1]*Energy Resources and Petroleum Engineering, King Abdullah University of Science and Technology, Thuwal 23955-6900, Saudi Arabia*
[2]*Craft & Hawkins Department of Petroleum Engineering, Louisiana State University, Baton Rouge 70803, United States of America*
[3]*Key Laboratory of Unconventional Oil and Gas Development, China University of Petroleum (East China)), Qingdao 266580, P. R.China*
[4]*State Key Laboratory of Oil and Gas Reservoir Geology and Exploitation, Southwest Petroleum University, Chengdu 610000, P. R. China*

Keywords:
Numerical simulation
geological carbon storage
solubility trapping
WAG injection
complex reservoirs

Cited as:
Tariq, Z., Estrada, J. K. P., Yan, B., Xu, J. Numerical investigation of CO_2 solubility trapping mechanisms for enhanced storage in saline aquifers. Computational Energy Science, 2024, 1(4): 175-187. https://doi.org/10.46690/compes.2024.04.03

Abstract:
Geological Carbon Storage (GCS) faces significant challenges related to the potential leakage of CO_2 through cap rocks, posing risks of contamination to drinking resources and disruption to various ecosystems. Therefore, it is essential to develop and implement optimal injection strategies to minimize CO_2 escape from the formation. This study evaluates the effectiveness of three distinct CO_2 injection strategies in complex saline aquifers: pure supercritical CO_2 (SC-CO_2), carbonated water (CW), and Water-Alternating-Gas (WAG). The results demonstrate that SC-CO_2 injection primarily relies on structural trapping, complemented by residual trapping and a minor contribution from solubility trapping. In contrast, CW injection significantly enhances solubility trapping to nearly complete levels, while structural and residual trapping are minimized. On the other hand, WAG injection strategies, characterized by varying cycle frequencies, exhibit a balanced trapping profile, with solubility trapping progressively increasing while maintaining structural and residual mechanisms to support overall storage. Previous studies have shown that SC-CO_2 injection efficiently fills pore spaces and displaces resident brine within the storage formation. However, the buoyant nature of CO_2 remains a challenge to secure long-term storage efficiency. CW injection emerges as a promising alternative by leveraging the solubility of CO_2 in resident brine. Dissolving CO_2 in water prior to injection mitigates gravity segregation between brine and CO_2, thereby improving volumetric sweeping efficiency within the formation. Additionally, WAG injection offers potential benefits by dynamically alternating SC-CO_2 and water phases to enhance trapping and immobilization. Nevertheless, both CW and WAG injection strategies face challenges related to operational costs. CW injection requires a substantial volume of water to dissolve CO_2, while WAG injection demands meticulous monitoring and precise control, resulting in increased energy consumption-particularly when highly compressed CO_2 is needed. These factors collectively contribute to the elevated cost of CW and WAG injection strategies, highlighting the need for further optimization to enhance their economic viability.

1. Introduction

Fossil fuels including coal, oil, and natural gas have long been the backbone of the global economy, serving as the primary energy source for decades (Miguel et al., 2018). However, their extensive use has significantly increased emissions of CO_2 and other greenhouse gases, accelerating climate change and environmental degradation (Holt and Lindeberg, 1992). To mitigate these emissions, Carbon Capture, Utilization, and Storage (CCUS) has emerged as a promising technology (Vilarrasa and Rutqvist, 2017). According to the International Energy Agency (IEA), CCUS could contribute to a 17% reduction in global CO_2 emissions by 2050 (Raza et al., 2019). CCUS involves capturing CO_2 from large-scale point sources (e.g., power plants), followed by uti-

Yandy Scientific Press

*Corresponding author.
E-mail address: zeeshan.tariq@kaust.edu.sa (Z. Tariq); bicheng.yan@kaust.edu.sa (B. Yan); jpauya1@lsu.edu (J. K. P. Estrada); xujianchun@upc.edu.cn (J. Xu); youweihe_cupb@163.com (Y. He).

Received October 9, 2024; revised November 13, 2024; accepted December 13, 2024; available online December 16, 2024.

lization, transportation, and injection into geological formations for long-term sequestration (GLOBAL, 2023). Potential storage sites include saline aquifers, depleted hydrocarbon reservoirs, and coal seams (Hassanzadeh et al., 2009; Motie and Assareh, 2020; Alkan et al., 2021). While geological CO_2 sequestration (GCS) has been studied since the early 1990s, challenges such as storage risks, costs, and large-scale site availability remain significant barriers to implementation (Leonenko and Keith, 2008). Addressing even one-third of current global CO_2 emissions through CCUS would require storing CO_2 at an average rate of 15 km^3/year at reservoir conditions-5,000 times the total volume currently injected in worldwide CCS projects (Leonenko and Keith, 2008). This highlights the immense scale required for CCUS to have a meaningful impact on climate mitigation.

Among the available geological formations, deep saline aquifers offer significant storage potential due to their vast capacity and multiple trapping mechanisms (Leonenko and Keith, 2008; Grobe et al., 2009; Ajayi et al., 2019). CO_2 can be retained through four primary mechanisms: structural trapping, where CO_2 accumulates beneath impermeable caprocks; solubility trapping, where CO_2 dissolves into resident brine; residual trapping, where CO_2 is immobilized within rock pores at irreducible gas saturation; and mineral trapping, where CO_2 reacts with host minerals to form stable carbonate precipitates (Hassanzadeh et al., 2009; Nghiem et al., 2009). Despite these mechanisms, buoyancy remains a key challenge, as supercritical CO_2 (SC-CO_2) is 10-40% less dense than brine, leading to lateral migration and potential leakage through caprocks (Leonenko and Keith, 2008; Hassanzadeh et al., 2009).

To enhance CO_2 storage efficiency and mitigate buoyancy-driven migration, alternative injection strategies have been proposed, including carbonated water (CW) and Water-Alternating-Gas (WAG) injection (Jikich et al., 2003). CW injection, initially developed for Improved Oil Recovery (IOR), involves dissolving CO_2 in water before injection. This approach enhances CO_2 dissolution, reduces gravity segregation, and improves volumetric sweep efficiency (Jikich et al., 2003). Meanwhile, WAG injection, originally introduced as an Enhanced Oil Recovery (EOR) method, cycles between CO_2 and water slugs to enhance residual trapping, promote dissolution, and control plume migration (Agarwal and Zhang, 2014). While WAG improves storage efficiency, its higher operational complexity and cost implications require further optimization.

Traditionally, pure CO_2 is injected in its supercritical phase due to its advantages in solubility and wellbore stability. SC-CO_2 dissolves more readily in brine than gaseous CO_2 and prevents hydrate formation, which can obstruct injection wells (Foroozesh and Jamiolahmady, 2018). However, the high buoyancy-driven mobility of SC-CO_2 can result in inefficient storage and increased leakage risk. CW and WAG injection strategies have been developed to counter these issues. CW injection improves solubility trapping, while WAG enhances residual and solubility trapping through cyclic water injection (Jikich et al., 2003). CW injection was initially introduced for improved oil recovery (IOR), where injecting CO_2-saturated water facilitates CO_2 dissolution while reducing gravity segregation effects (Jikich et al., 2003). Similarly, WAG injection, originally developed for enhanced oil recovery (EOR), involves the alternating injection of water and CO_2 to mobilize residual hydrocarbons. Beyond oil recovery, researchers have demonstrated that WAG injection can significantly enhance CO_2 storage efficiency by reducing plume migration, improving residual trapping, and accelerating CO_2 dissolution (Agarwal and Zhang, 2014). Although additional water injection increases operational costs, WAG remains a promising technique for optimizing long-term CO_2 sequestration.

In geological sequestration, the mobility ratio between the non-wetting phase (CO_2) and the wetting phase (brine) is a critical parameter for optimizing injection efficiency. The mobility ratio is defined as:

$$M = \frac{m_n}{m_w} = \frac{\mu_w k_{rw}}{\mu_n k_{rw}} \tag{1}$$

where μ_w and μ_n are the viscosities of the wetting phase and non-wetting phase, respectively; k_{rw} and k_{rn} are the relative permeabilities of the wetting phase and non-wetting phase, respectively. When $M < 1$, the displacement of the resident wetting phase (brine water) by the injected non-wetting phase is stable, otherwise, inefficient displacement occurs due to the formation of water/gas fingers.

Considering the intermittent CO_2-water injection as a pseudo-mixture entering the aquifer during WAG injection, the mobility ratio would be lower than that of pure CO_2 injection. Moreover, the mobility ratio determines the velocity for buoyancy-driven CO_2 migration (Agarwal and Zhang, 2014). The enhanced CO_2 dissolution is also a favorable characteristic of the WAG technique. Numerous studies have been conducted to accelerate CO_2 dissolution by injecting brine into the aquifer after CO_2 injection (Bryant et al., 2008; Leonenko and Keith, 2008; Orr, 2010; Agarwal and Zhang, 2014), and promising results have been obtained from numerical simulations and feasibility analysis (Leonenko and Keith, 2008; Agarwal and Zhang, 2014).

Since CO_2 is more soluble in water than other gases (Sohrabi et al., 2011), CW has also attracted significant attention in GCS. This strategy offers the dual benefit of utilizing the injected CO_2 for EOR and GCS purposes (Sohrabi et al., 2008; Burton and Bryant, 2009; Motie and Assareh, 2020), and reducing costs related to CO_2 capture and pressurization (Sohrabi et al., 2008; Burton and Bryant, 2009). Previous studies showed that CW injection has been an attractive strategy as a flooding agent for more than half a century, improving its efficiency in both lab and field scales (Foroozesh and Jamiolahmady, 2018; Esene et al., 2019; Sadati et al., 2020). Additionally, CW can eliminate many deficiencies of pure supercritical CO_2 injection, e.g., poor volumetric sweeping efficiency due to the high mobility of CO_2 (Esene et al., 2019). When injecting water with dissolved CO_2 for EOR purposes, the dissolved CO_2 transfers from the injected water to the oil phase, leading to a more gradual front of CO_2 than the water front. Due to density contrasts and lower CO_2 mobility in carbonated water, CW injection considerably enhances the sweeping efficiency and thus displaces more oil than water-flooding or pure CO_2 injection (Foroozesh and Jamiolahmady, 2018). What is more, CW presents a lower risk of gravity-driven leakage, as brine with dissolved CO_2 naturally sinks and remains at the bottom

of the injection region due to gravity. Furthermore, CW is still feasible even with insufficient CO_2 sources (Sohrabi et al., 2008; Burton and Bryant, 2009; Alizadeh et al., 2014; Bisweswar et al., 2020; Motie and Assareh, 2020). However, a critical drawback arises from CO_2's limited solubility in water: although this property reduces the absolute CO_2 volume required for injection (Foroozesh and Jamiolahmady, 2018), dissolving substantial amounts of CO_2 necessitates large water volumes, significantly increasing operational costs (Bryant et al., 2008; Burton and Bryant, 2009). Despite this trade-off, CW remains a pragmatic compromise between efficiency, cost, and environmental safety.

To safely contain CO_2 in aquifer, it is essential to understand the multiphase fluid flow processes occurring in storage reservoirs. In this study, the process of CO_2 injection for geological sequestration is simulated using the physics-driven simulator CMG-GEM (Tariq et al., 2023), which models CO_2 behavior from surface injection to long-term storage, allowing for detailed monitoring of plume migration over time.

2. Methodology

The primary goal of this research is to explore and analyze various CO_2 injection strategies aimed at enhancing the sequestration of CO_2 through increased solubility trapping within saline aquifers. The study delves into three distinct scenarios to assess their effectiveness in achieving this objective. The first scenario is the injection of supercritical CO_2 (SC-CO_2); the second scenario is the injection of carbonated water (CW), which indicates brine with dissolved CO_2; the third scenario is cyclic CO_2-brine injection, commonly known as WAG. Additionally, the research investigates five variations of cyclic injection in the WAG scenario, including scenarios WAG with 1, 2, 3, 5, and 6 cycles, respectively.

To prevent excessive pressure buildup in the reservoir during CO_2 injection, a volume multiplier of 10^6 was applied at the lateral boundaries to simulate an infinite aquifer boundary condition. This adjustment mitigates pressure escalation and ensures stable injection conditions with low risk of cap-rock failure. The effect of this volume multiplier is particularly significant in CW injection due to its higher viscosity compared to SC-CO_2, leading to a more pronounced pressure increase at the bottomhole.

2.1 Model description

We take the GCS model from the 11th SPE Comparison Solution (11th SPE CSP) (SPE, 2023) in this work. Fig. 1 illustrates the sketch of the model. The reservoir is in the shape of anticline closure which elevates the central part of the domain by 150 m^3. The formation size is 8,400 × 5,000 × 1,200 m^3 along the x, y, and z-axis, respectively. The reservoir domain is discretized by a corner point grid system to honor the reservoir geometry, with in total 86 × 50 × 60 = 25,800 grid blocks along the x, y, and z-axis, respectively. The model presents two reservoir formations, each overlaid by a cap-rock with a very low permeability. The top of the lower and upper storage formations is at depths of 1,900 and 4,200 meters, respectively.

The reservoir is initially fully saturated with water with a salinity equal to 57,000 ppm. The model is initially in hydrostatic equilibrium with an initial pressure at the top of the geometry equal to 196 bar. The reservoir has no-flow boundary conditions, and at the left and right boundary of the model, a pore volume multiplier is applied in order to avoid unphysical pressure increment, as specified in the 11th SPE CSP model description (SPE, 2023).

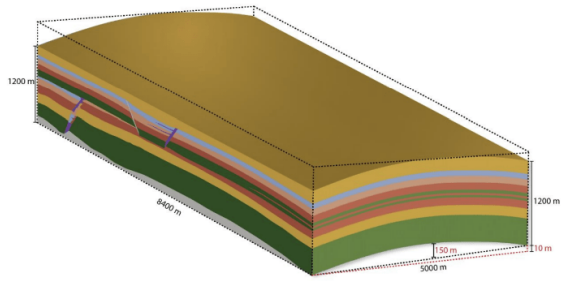

Fig. 1. Sketch of the Geometry for the CSP11C Case (SPE, 2023).

Two horizontal injection wells are considered. The horizontal part of the first injection well INJ0 follows the bending of the anticline, which is perforated between the points (5,100, 1,000, 700) meters and (5,100, 4,000, 700) meters. The horizontal part of the second well INJ1 is straight horizontal, which is perforated between the points (2,700, 1,000, 300) meters and (2,700, 4,000, 300) meters. Supercritical CO_2 is injected at the temperature of 40 °C and a maximum bottomhole pressure equal to 400 bar. As a result, if the injection pressure exceeds 400 bar, the well will be shut-in to stop the injection.

Three different CO_2 injection strategies are assessed: SC-CO_2 injection, CW injection, and five WAG scenarios (1, 2, 3, 5, and 6 cycles). The simulation ensures comparability by maintaining an equal cumulative injection of CO_2 and brine across all cases. Each WAG cycle consists of alternating CO_2 and brine injection phases, with the duration of each phase adjusted to distribute the total 30-year injection period equally among the cycles. For instance, in the 1-cycle WAG scenario, each injection phase lasts 15 years; for 2 cycles, each phase is 7.5 years; for 3 cycles, 5 years; for 5 cycles, 3 years; and for 6 cycles, 2.5 years.

As seen in Fig. 2, there are two permeable porous storage formations in the model, which are separated by an impermeable layer, and the upper reservoir is overlaid by another impermeable layer. Thus, to store CO_2 efficiently, two horizontal wells are perforated in each of the permeable formations: the well INJ0 is located in the lower storage formation, while the well INJ1 is perforated in the upper storage formation. Moreover, it is imperative to notice that the model presents four fault, as seen in Fig. 2(a). In order to make all injection scenarios comparable, the same (cumulative) amount of CO_2 and brine is injected over the whole injection time. Table 1 shows the injection parameters for all cases.

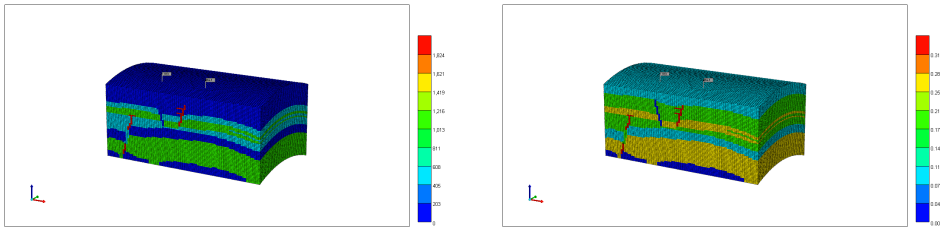

(a) (b)

Fig. 2. Reservoir properties: (a) horizontal permeability; (b) porosity.

Table 1. Model injection parameters.

Parameter	SC-CO_2	CW	WAG 1 cycle	WAG 2 cycles	WAG 3 cycles	WAG 5 cycles	WAG 6 cycles
Max BHP [bar]	400	400	400	400	400	400	400
CO_2 mass rate per well [Mton/y]	1.317	1.317	2.634	2.634	2.634	2.634	2.634
Water mass rate per well [Mton/y]	-	43.8	87.6	87.6	87.6	87.6	87.6
Injected cumulative CO_2 per well [Mton]	39.501	39.501	39.501	39.501	39.501	39.501	39.501
Injected cumulative water per well [Mton]	-	1314	1314	1314	1314	1314	1314
Total amount of pore volume injected (both wells)	5.082 E-3 PV	3.150 E-4 PV	5.398 E-3 PV	5.398 E-3 PV	5.398 E-3 PV	5.398 E-3 PV	5.398 E-3 PV

2.2 Relative permeability and capillary pressure

In this work, the relative permeability and capillary pressure functions for each facie in the model obeys the Brook-Corey correlation as specified in the spe11c description (SPE, 2023), and the formulation will not be repeated here. Fig. 3 shows the relative permeability and capillary pressure functions, respectively

2.3 CO_2 solubility in aqueous phase

The equation of state (EOS) used in this work is the well known Peng-Robinson (PR) to calculate the CO_2 thermodynamic properties.

Since the CO_2 solubility in the aqueous phase is a quick process, a thermodynamic equilibrium between the gas and aqueous phases can be assumed, as shown in Eq. 2:

$$f_{ig} - f_{iw} = 0, \quad i = 1, 2, ..., n_g \tag{2}$$

where f_{ig} and f_{iw} are the component i fugacities in the gas and aqueous phases.

f_{ig} is calculated from the PR EOS while f_{iw} uses Henry's law that relates the fugacity of a component to its concentration as shown in Eq. 3:

$$f_i = x_{iw} * H_i \tag{3}$$

where x_{iw} is the mole fraction of component i in the liquid phase, H_i is Henry's constant, which is a function of pressure, temperature, and aqueous phase salinity.

Thus, since CO_2 solubility in the aqueous phase plays a significant role, it is crucial to know the amount of CO_2 dissolved (CO_2 concentration) in the aqueous phase under certain pressure and temperature conditions. The United States Geological Survey has developed a software called PHREEQC to calculate the CO_2 solubility in the aqueous phase, as seen in Fig. 4.

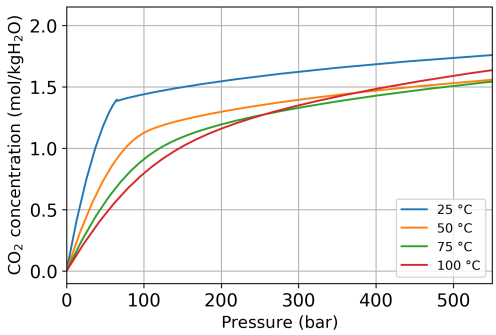

Fig. 4. CO_2 solubility at high pressures with no salinity (Parkhurst and Appelo, 2013).

Fig. 4 shows the comparison between experimental data (points) and the simulator PHREEQC (solid lines). The data

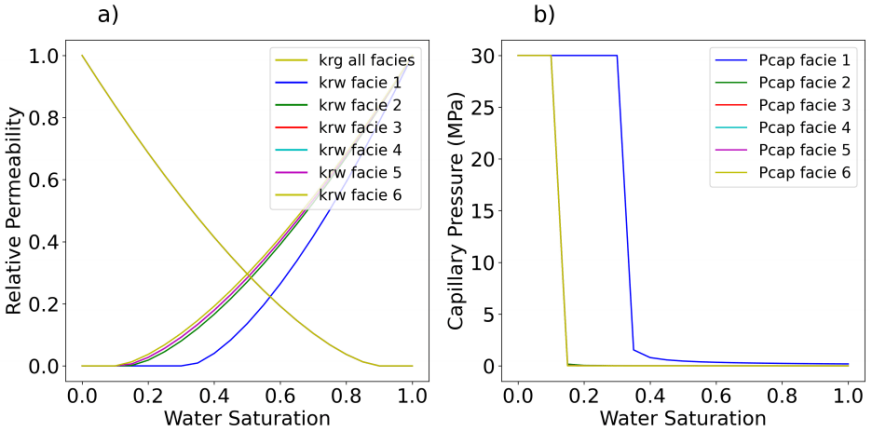

Fig. 3. Brooks-Corey relative permeability (a) and capillary pressure (b) for each facie.

points were taken from experimental data provided by Duan et al. (2006), and Spycher et al. (2003). As mentioned previously, one of the cases studied in this work is the co-injection of CO_2 and brine (CW), thus, it is crucial to know the CO_2 concentration (molality) in brine so that 100% of the injected CO_2 will be dissolved in the aqueous phase (injected brine). Fig. 5 shows the CO_2 molality dissolved in water with different salinity (0 and 2 molal) at different pressures and temperatures calculated using PHREEQC.

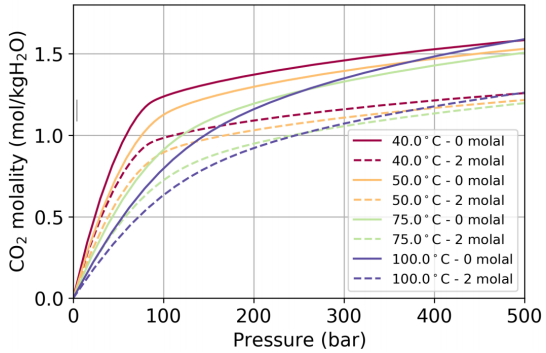

Fig. 5. CO_2 solubility comparison with no salinity and salinity.

As seen from Fig. 5, it can be seen that the CO_2 solubility increases when increasing the pressure but decreases as temperature and salinity of the water increases. This behavior was previously reported by (Sadati et al., 2020; Addassi et al., 2021).

3. Governing Equations

Several studies showed that when supercritical CO_2 is injected into a deep saline aquifer, a two-phase fluid flow is created (brine-CO_2) (Celia et al., 2015; Zamani et al., 2024). The CO_2 is slightly miscible with the brine with up to a few percent by mass dissolving into the brine, and an even smaller H_2O fraction (less than 1 %) can evaporate into the CO_2 phase (Celia et al., 2015).

When CO_2 dissolves into the resident brine, the pH of the aqueous phase decreases, driving a sequence of geochemical reactions in the saline aquifer and aquitard rocks and in well cements. Similarly, H_2O partitions into the CO_2-rich phase creates "wet" CO_2, which can be much more corrosive to metal piping compared to "dry" CO_2 (Celia et al., 2015).

3.1 Mass balances and constitute equations

CO_2-brine system involves basic balance equations, written either for the bulk phases or for the major components of the phases. The mass balance equation for each component in the system is described by Eq. 4 (Celia et al., 2015):

$$\sum_{\alpha}\left[\frac{\partial(\rho_\alpha \phi s_\alpha m_\alpha^i)}{\partial t}+\nabla(\rho_\alpha u_\alpha m_\alpha^i + j_\alpha^i)\right]=\sum_{\alpha}\psi_\alpha^i \quad (4)$$

where ρ_α is the density of the phase α, ϕ is the porosity, s_α is the saturation of the fluid phase α, m_α^i is the mass fraction of component i in the phase α, u_α is the volumetric flux vector (Darcy flux) for phase α, j_α^i is the non-advective flux vector (diffusion and mechanical dispersion) for component i in phase α, ψ_α^i is the external sources or sinks of mass for component i in phase α. In the equation, components represent CO_2, H_2O, NaCl, and others if any $i = CO_2, H_2O, NaCl, \ldots$ and phases called brine and CO_2.

The mass balance equation needs to be augmented by constitutive equations and equations of state, including the multiphase extension of Darcy's equation (Celia et al., 2015):

$$u_\alpha = -\lambda_\alpha k(\nabla p_\alpha - \rho_\alpha g) \quad (5)$$

where $k_{r,\alpha}$ is the relative permeability, taken as a scalar and a function of the phase saturation s_α, k is the intrinsic permeability tensor, μ_α is the phase viscosity, λ_α is the phase mobility, p_α is the phase pressure, g is the gravitation acceleration vector directed downward with the positive vertical direction pointed upward.

Additional equations include:

$$\sum_{\alpha} m_\alpha^i = 1 \quad (6)$$

$$\sum_{\alpha} s_\alpha^i = 1 \quad (7)$$

3.2 Equations for horizontal wells

Horizontal wells can greatly improve both injectivity and storage capacity, as well as lead to a higher CO_2 dissolution

rate compared to the vertical injection well when water-chasing injection is applied.

In CMG, for a horizontal well, the wellbore (flowing bottomhole) and the pressure at the grid block containing the well are related by the Eq. (8) (Peaceman, 1993):

$$p_{wf} = p_o - \frac{q\mu}{2\pi(k_x k_z)^{1/2}\Delta y} \ln \frac{r_o}{r_w} \tag{8}$$

For an an anisotropic medium:

$$r_o = \frac{0.14(k_z/k_x)^{1/2}\Delta x^2 + (k_x/k_z)^{1/2}\Delta z^2}{0.5[(k_z k_x)^{1/4} + (k_x/k_z)^{1/4}]} \tag{9}$$

4. Results and discussions

4.1 Efffect of carbonated brine injection

Fig. 6 illustrates the global CO_2 mole fraction within the horizontal (XY) and vertical (YZ) planes across the storage porous formations, considering both pure SC−CO_2 and CW injection scenarios for both horizontal wells. For both cases, the injection rate of CO_2 and brine for both wells is equal to 1.93×10^7 mol/d (about 1.32 MMton/y) and 1.2×10^8 kg/d (about 43.8 MMton/y), respectively.

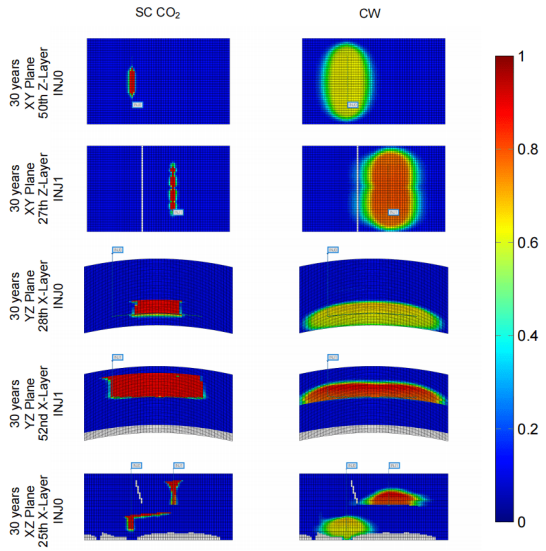

Fig. 6. Global CO_2 mole fraction for the SC-CO_2 and CW injection cases for both INJ0 and INJ1 horizontal wells after 30 years in XY, YZ, and XZ planes.

Additionally, since a small section of the well INJ1 is perforated in a low-permeability zone ($K_i = 0.1$ mD) as seen from Fig. 2(a), a slight leakage can be seen in Fig. 6 (YZ plane) when injecting CW. However, this slight leakage does not happen when injecting SC-CO_2 since it tends to flow upwards due to gravity effects. From Fig. 2(a), a sealing fault can be seen in the upper storage formation where the well INJ1 is located. When injecting CW into the formation, the CO_2 plume reaches the sealing, not allowing the CO_2 to flow through it. However, the CO_2 can flow through neighboring lower cells, and thus, CO_2 plume can be seen on the left side of the sealing (XY and YZ planes). Furthermore, it is imperative to mention that CO_2 follows the permeability distribution along the storage formations easier when injection injecting pure SC-CO_2 than CW. Although supercritical CO_2 indeed combines characteristics of both liquids and gases, the CO_2 tends to exhibit a lower viscosity when it is injected pure rather than injecting it dissolved in the aqueous phase (carbonated water). This lower viscosity allows SC-CO_2 to flow through porous formations more readily, navigating the permeability distribution with reduced resistance. Thus, it can be seen in Fig. 6 from the XZ plane that the CO_2 plume follows the permeability field shown in Fig. 2(a) when injecting it pure through the horizontal well INJ0.

Since CW is basically water containing dissolved CO_2, it increases the amount of CO_2 that can be dissolved in the formation resident brine. Thus, as seen in Fig. 6, when injecting CW into a saline aquifer, the CO_2 spreads through a higher area than in the case of pure SC-CO_2. This can be seen in Fig. 7. Structural trapping arises from the behavior of free (buoyant) CO_2 nature during its injection into geological formations, being trapped within the geological structure of the reservoir. In other words, structural trapping relies on the CO_2 molecules becoming physically trapped in the pore space and, thus, forming structures that prevent their movement. In the context of the CW injection, where the CO_2 is already dissolved in brine prior to injection, the CO_2 buoyant nature is eliminated. However, as the CW solution flows from the surface to the subsurface formation, temperature changes - attributed to the geothermal gradient-may induce the release of CO_2 from the CW solution. For this reason, structural trapping contribution is significantly lower for the CW injection case, as seen in Fig. 7. Additionally, when CO_2 is injected in its supercritical state, the resident fluid in the storage formation is displaced as the CO_2 flows through the porous media, and small portions are left behind as residual droplets in the porous rock. Moreover, when injecting SC-CO_2, it tends to remain in this state, being more effectively trapped by capillary forces in the pore space. In contrast, the injected CW is more mobile and, thus, may not be effectively trapped in the pore space over the long term. Fig. 7 shows that the CO_2 residual trapping contribution is significantly less for the CW case than for the SC-CO_2 case.

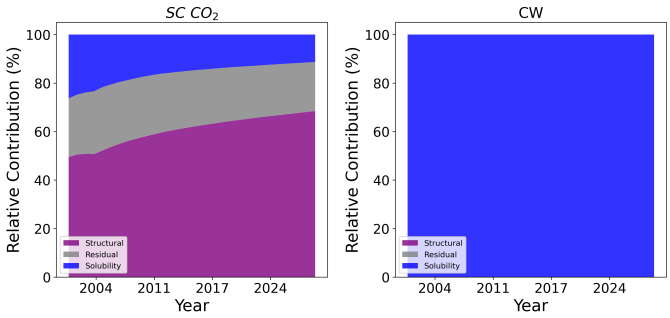

Fig. 7. CO_2 trapping mechanisms relative contribution for both SC-CO_2 and CW injection cases.

Table 2 shows the quantity of CO_2 trapped by solubility, structural, and residual mechanisms for the SC-CO_2, and CW injection cases.

Table 2. Amount of CO_2 trapped by different mechanisms for the SC-CO_2 and CW cases after 30 years of continuous injection.

Trapping mechanism	SC-CO_2	CW
Structural (Supercritical CO_2)	7.710E11 mol	1.601E7 mol
Residual (Trapped CO_2)	2.275E11 mol	1.601E7 mol
Solubility (Dissolved CO_2)	1.277E11 mol	8.978E11 mol

4.2 Effect of Water-Alternating-Gas (WAG) injection

In this work, the WAG method was also studied for GCS in saline aquifer for two horizontal wells. Five cases were simulated: i) WAG injection with one cycle, ii) WAG injection with two cycles, iii) WAG injection with three cycles, iv) WAG injection with five cycles, and v) WAG injection with six cycles. One complete cycle is when SC-CO_2 injection is followed by brine injection. For simplicity, we set that each cycle is identical with equal time of injection phase. Fig. 8 represents a schematic representation of the considered WAG injection.

In this section, we focus on only the first scenario case (WAG injection with one cycle) to compare it to the baseline case of SC-CO_2 injection. And, in the next section, the impact of the number of cycles on the global CO_2 mole fraction will be studied.

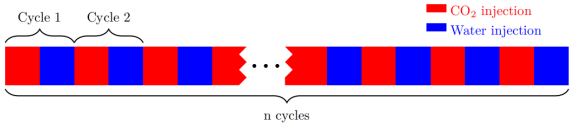

Fig. 8. WAG injection schematic representation.

In order to make WAG case comparable to the previous ones (SC-CO_2 and CW), the same amount of CO_2 and water (cumulative) should be injected over the whole injected period (30 years). Thus, the rate of the injected CO_2 and brine for both cyclic cases is equal to 1.64×10^8 mol/d (about 2.64 MMton/y) and 2.4×10^8 kg/d (about 87.6 MMton/y), respectively through each well.

Fig. 9 presents the global CO_2 mole fraction within the horizontal (XY) and vertical (YZ and XZ) planes across the storage zone, comparing scenarios of the SC-CO_2, and WAG with one cycle. Fig. 9 shows that the WAG injection enhances the sweeping efficiency of CO_2 along the storage zone, reaching a higher distance in comparison with the pure SC-CO_2 case, but a lower distance than when injecting CW. When injecting brine cyclically after CO_2 (two phases and not one as in the CW injection case), it can be clearly observed that the buoyancy effect of the CO_2 plume is minimized. In the case of WAG injection with one cycle, SC-CO_2 is injected for the first 15 years, and then, brine is injected for the following 15 years.

During the pure SC-CO_2 injection phase, the CO_2 tends to accumulate in the upper part of the perforated section of the well INJ0, but then, when the brine injection phase starts, the water minimizes the segregation effect of the previously injected SC-CO_2, and displaces the CO_2 from the near-wellbore zone to the upper part of the formation. Moreover, as explained before, the water improves the CO_2 dissolution and sweeping efficiency, making the CO_2 plume reach a further horizontal distance as seen from YZ and XZ planes.

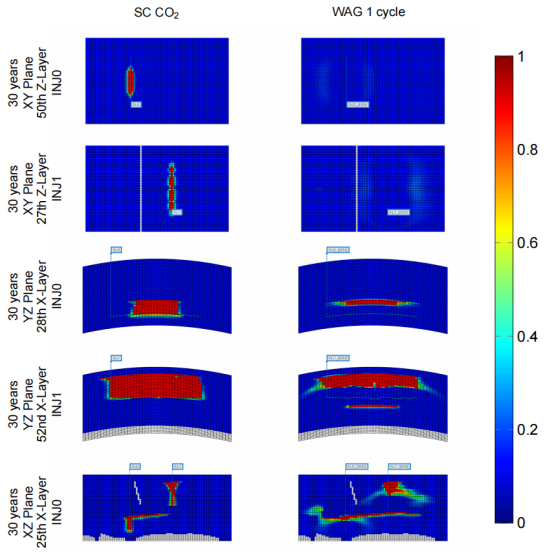

Fig. 9. Global CO_2 mole fraction for the SC-CO_2 and WAG with one-cycle cases for both INJ0 and INJ1 horizontal wells after 30 years in XY, YZ, and XZ planes.

Moreover, similar to the SC-CO_2 case, the CO_2 plume in the WAG with one cycle case also follows the high-permeability channels. As seen in Fig. 2(a), the lower and upper storage zones are connected through a tiny channel in the left part of the reservoir domain. Since the brine injection leads to an improved CO_2 sweeping efficiency, the CO_2 plume reaches a longer horizontal distance, flowing from the lower to the upper formations. Depending on the injection rate, a higher or lower amount of CO_2 will flow from the lower to the upper formation.

Fig. 10 shows the relative contribution of the different CO_2 trapping mechanisms (structural, residual, and solubility) over time for the supercritical CO_2, CW, and WAG with single cycle cases. From Fig. 10, it can be seen that the CW injection case brings highest solubility trapping but lowest structural trapping since the CO_2 prior to injection is comprehensively dissolved in the aqueous phase eliminating the buoyancy effects, improving the storage efficiency. As mentioned previously, in order to make all cases comparable, the same amount of CO_2 (cumulative) should be injected over the whole simulation time (30 years), thus, the injection rate for the WAG injection case with one cycle is twice the rate for the pure SC-CO_2 case. For this reason, even though pure SC-CO_2 is injected during the first 15 years, a higher amount of CO_2 is trapped in the formation (higher solubility trapping). Then, as the subsequent 15-year phase of pure brine injection starts, it improves the CO_2 dissolution into the in-situ formation brine, significantly increasing the solubility trapping. As for the other two cases, during the first 15 years of continuous injection, the structural

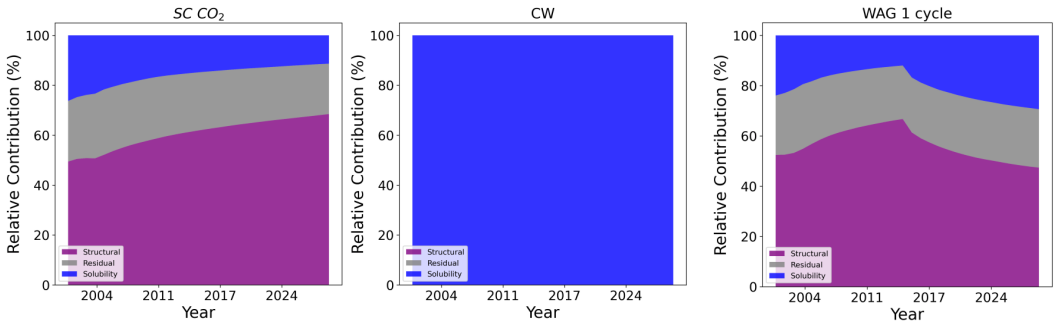

Fig. 10. Relative contributions of different CO_2 trapping mechanisms for the SC-CO_2, CW, and WAG with a single cycle cases.

trapping is higher for the cyclic case than for the pure SC-CO_2, even though pure SC-CO_2 is injected for both cases in this period. This is because the injection rate for the cyclic case is twice the rate for the pure SC-CO_2, leading to a higher amount of buoyant SC-CO_2 in the formation. On the other hand, as brine injection starts for the cyclic case for the subsequent 15 years, the CO_2 in the reservoir is displaced, and its buoyancy nature is minimized by the injected brine, decreasing the amount of free CO_2 in the storage formation, being slightly lower than for the pure SC-CO_2 case, as seen from Fig. 10.

Fig. 10 shows the CO_2 residual trapping mechanism for all cases studied in this section, being the lowest for the CW case. For the first 15 years, the residual trapping is higher for the cyclic case than for the SC-CO_2 case, since more CO_2 is injected. Then, as the brine injection phase occurs for the subsequent 15 years, the residual trapping decreases. This is because the brine improves the CO_2 dissolution into the formation brine, altering the phase behavior of CO_2 and potentially reducing its ability to be trapped in the pore spaces.

Table 3 shows the quantity of CO_2 trapped by solubility, structural, and residual mechanisms for the SC-CO_2, CW, and WAG with single cycle injection scenarios.

4.3 Effect of WAG injection with multiple cycles

Previously, we explored the effect of WAG injection with a single cycle on various CO_2 trapping mechanisms, with a specific emphasis on solubility trapping. In this section, we extend our investigation to encompass different injection strategies with multiple cycles. Specifically, four additional cases are studied, characterized by 2, 3, 5, and 6 cycles. The objective is to assess the impact of the number of injection cycles on the efficacy of trapping mechanisms.

Fig. 11 presents the global CO_2 mole fraction within the horizontal (XY) and vertical (YZ and XZ) planes across the storage porous zones, considering the WAG with 1, 2, 3, 5, and 6 cycles cases for both horizontal wells. From the plane XY in Fig. 11, when injecting the fluid through both wells, it can be seen that the CO_2 global mole fraction increases in the near-wellbore area. This phenomenon can be attributed to the increased number of cycles, leading to a reduction in the duration of each cycle. This shortened cycle time allows for more frequent injections of pure supercritical CO_2 and brine, contributing to the observed rise in the CO_2 concentration near the wellbore area. Consequently, with an increased frequency of pure CO_2 injections, there is a corresponding accumulation of CO_2 in the near-wellbore regions. Furthermore, a higher number of brine injections results in the CO_2 plume traveling a greater distance from the well, attributed to an improved CO_2 sweeping efficiency, as illustrated in the preceding section. Thus, the more times pure CO_2 is injected, the more it accumulates in the near-wellbore region. Additionally, the more times brine is injected, the CO_2 plume travels a further distance from the well due to an enhanced CO_2 sweeping efficiency, as demonstrated in the previous section.

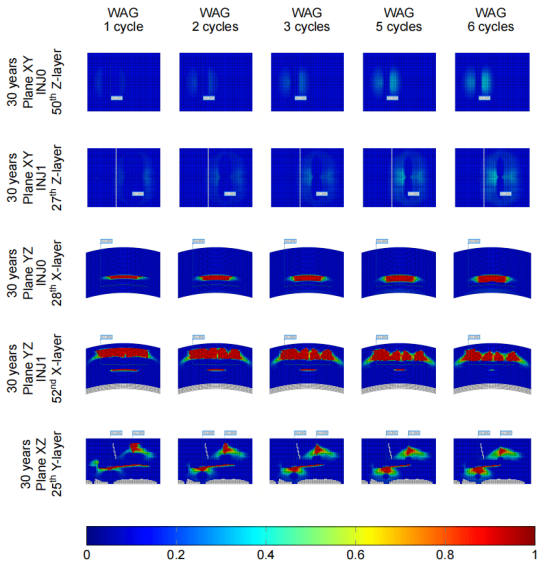

Fig. 11. Global CO_2 mole fraction for the WAG case with 1, 2, 3, 5, and 6 cycles for both INJ0 and INJ1 horizontal wells after 30 years in XY, YZ, and XZ planes.

Moreover, from the plane XZ, for the WAG case with a single cycle, it can be seen that the CO_2 flows from the lower to the upper formation through the interconnected permeable region when injected through the well INJ0, as seen in Fig. 6 and Fig. 11. However, this behavior is minimized when increasing the number of cycles. When injecting brine more frequently, the buoyancy effects of the CO_2 are diminished. Consequently, CO_2 tends to settle at the bottom due to gravity segregation with brine, leading to a reduction in the amount

Table 3. Amount of CO_2 trapped by different mechanisms for the SC-CO_2, CW, and WAG with 1 cycle injection cases after 30 years of continuous injection.

Trapping mechanism	SC-CO_2	CW	WAG-1 cycle
Structural (Supercritical CO_2)	7.71E11 mol	1.60E7 mol	5.54E11 mol
Residual (Trapped CO_2)	2.27E11 mol	1.60E7 mol	2.71E11 mol
Solubility (Dissolved CO_2)	1.27E11 mol	8.97E11 mol	3.43E11 mol

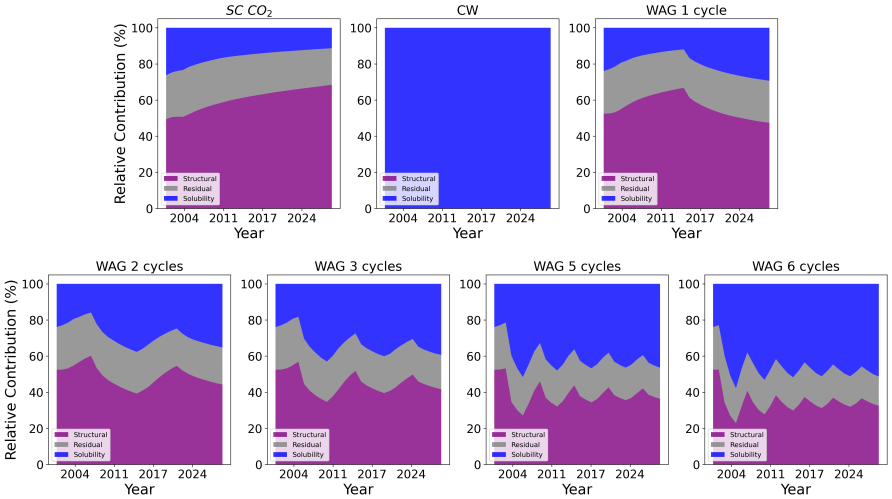

Fig. 12. CO_2 trapping mechanisms relative contribution for the SC-CO_2, CW, and WAG with 1, 2, 3, 5, and 6 cycles injection cases.

of buoyant SC-CO_2 in the upper part of the lower storage formation. This behavior is further evident in the YZ plane when injecting fluids through the horizontal well INJ1, where the global CO_2 mole fraction exhibits a decrease in the upper sections of both the upper and lower formations.

Fig. 12 shows relative contribution of the different CO_2 trapping mechanisms (structural, residual, and solubility) over time. It can be seen that the contribution of the solubility trapping is the highest for the CW injection case since the injected aqueous phase eliminates the buoyancy effects, improving the storage efficiency. For the cyclic cases, since the CO_2 mass rate is two times higher than for the SC-CO_2, a higher amount of CO_2 is trapped in the formation brine (higher solubility trapping).

Moreover, to gain a clearer understanding of the cyclic cases, we will segment the 30 years of continuous injection into twelve distinct frames, each lasting 2.5 years. During the initial 2.5-year period, where all cyclic cases involve CO_2 injection exclusively, the solubility trapping mechanism remains consistent. However, as the subsequent 2.5-year phase begins, the case with six cycles introduces the injection of brine. This results in a notably higher quantity (sharper increment of CO_2 being dissolved into the formation brine compared to the other cyclic cases, where pure SC-CO_2 injection persists, except for the case with 5 cycles. In this instance, the brine injection initiates after 3 years, leading to a slightly higher solubility trapping than the case with 6 cycles. This pattern continues throughout the timeline, signifying that the injection of CO_2 contributes to an increment of the amount of dissolved CO_2 within the formation brine. Simultaneously, the introduction of brine injection leads to a sharper increment of the solubility trapping. At the end of 30 years of continuous injection, the trend becomes evident-the amount of dissolved CO_2 increases when the number of cycles increases.

In the context of structural trapping, a similar trend is observable. Fig. 12 shows that the contribution of the structural trapping is the lowest for the CW case. For the cyclic cases, specifically during the first 2.5 years of pure SC-CO_2 injection, the amount of free CO_2 trapped in the reservoir structure remains constant. However, when the brine injection phase starts, structural trapping decreases as the aqueous phase displaces the buoyant SC-CO_2 in the reservoir, enhancing CO_2 dissolution. Furthermore, another notable observation is that during the first (initial) pure SC-CO_2 injection phase, the structural trapping is considerably higher for all cyclic cases compared to the pure SC-CO_2 case. This is due to the significantly higher CO_2 injection rate for the cyclic cases compared to the pure SC-CO_2 case.

However, at the end of the whole injection period (after 30 years), Fig. 12 shows that the structural trapping contribution is the highest for the pure SC-CO_2 case since no brine is injected at all. For the cyclic cases, as explained before, when the brine injection phase starts, it increases solubility trapping but decreases the amount of buoyant SC-CO_2 in the reservoir, and thus, the structural trapping reduces. Additionally, it can be seen that the structural trapping decreases when the number of

Table 4. Amount of CO_2 trapped by different mechanisms for the SC-CO_2, CW, and WAG with 1, 2, 3, 5, and 6 cycles injection cases after 30 years of continuous injection. (Unit: mol)

Trapping mechanism	SC-CO_2	CW	WAG-1 cycle	WAG-2 cycles	WAG-3 cycles	WAG-5 cycles	WAG-6 cycles
Structural (Supercritical CO_2)	7.7107E11	1.6019E7	5.5418E11	4.9500E11	4.6277E11	3.9617E11	3.3753E11
Residual ((Trapped CO_2)	2.2755E11	1.6015E7	2.7161E11	2.2826E11	2.1052E11	1.8787E11	1.6845E11
Solubility ((Dissolved CO_2)	1.2778E11	8.9787E11	3.4324E11	3.9372E11	4.3775E11	5.0514E11	5.3273E11

cycles increases. This phenomenon is attributed to the higher frequency of brine injection following the phase of pure SC-CO_2 injection.

Furthermore, Fig. 12 shows the contribution of the residual trapping mechanism of CO_2, being the lowest for the CW case. The residual trapping is significantly higher for the cyclic cases compared to the pure SC-CO_2 case during the first CO_2 injection phase. This is because the injection rate for the cyclic case is twice the rate for the pure SC-CO_2 case.

Subsequently, similar to the observed trend for the CO_2 structural trapping mechanism, the quantity of CO_2 trapped in the porous space decreases during the brine injection phase. This can be attributed to the increased sweeping efficiency of CO_2 by the brine, and enhanced CO_2 dissolution within the formation brine. Fig. 12 underscores the impact of the number of cycles on the residual trapping. As the number of cycles increases, the amount of CO_2 trapped in the porous space decreases due to the higher frequency of displacement and dissolution of CO_2.

Table 4 shows the quantity of CO_2 trapped by solubility, structural, and residual mechanisms for all cases.

Fig. 13 supplements the insights from Fig. 12, providing a more nuanced understanding of each CO_2 trapping mechanism's contribution after 30 years of continuous injection. It can be clearly seen that the contribution of the solubility trapping is significantly higher for the CW case than for the SC-CO_2 case. And, when introducing the WAG injection, the solubility trapping increases as the number of cycles increments. In contrast, the pure SC-CO_2 case exhibits the highest degree of structural trapping, while the WAG case with a single cycle excels in residual trapping. Moreover, the amount of CO_2 trapped by both structural and residual mechanisms reduces as the number of cycles increases. For the case of the CW injection scenario, both structural and residual trapping mechanisms contribute little to the overall amount of trapped CO_2, playing a minor role, as seen in Fig. 13. Importantly, it is emphasized that the solubility trapping stands out as the primary contributor to GCS when injecting carbonated water into the storage formation. And, its contribution increases when incrementing the number of cycles for the WAG injection.

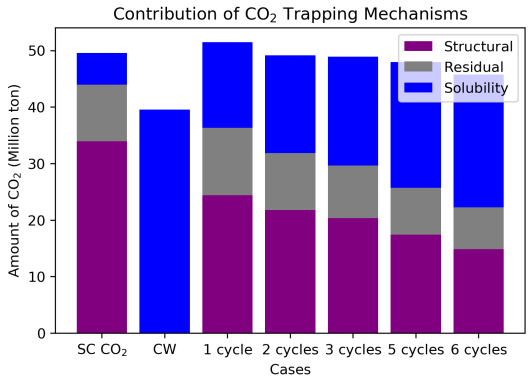

Fig. 13. Contribution of different CO_2 trapping mechanisms.

4.4 Impact on the bottomhole pressure

The injection of CO_2 into a saline aquifer significantly increases pressure in the vicinity of the wellbore. Depending on the injection rate, this pressure increment can be substantial and potentially damage the formation. To mitigate the risk of uncontrolled pressure buildup, a volume increment of 10^6 was applied at the lateral boundaries of the reservoir, effectively simulating an infinite aquifer, as seen in Fig. 14.

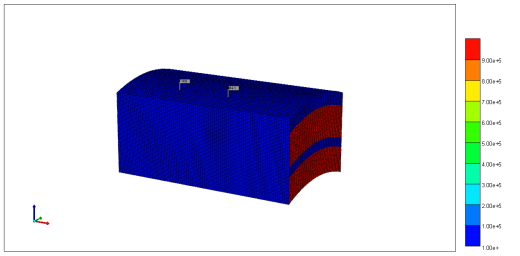

Fig. 14. Volume multiplier.

With the incremental volume at the lateral boundaries by 10^6, the pressure experiences a slight increase during the injection of pure Supercritical CO_2 (SC-CO_2), remaining

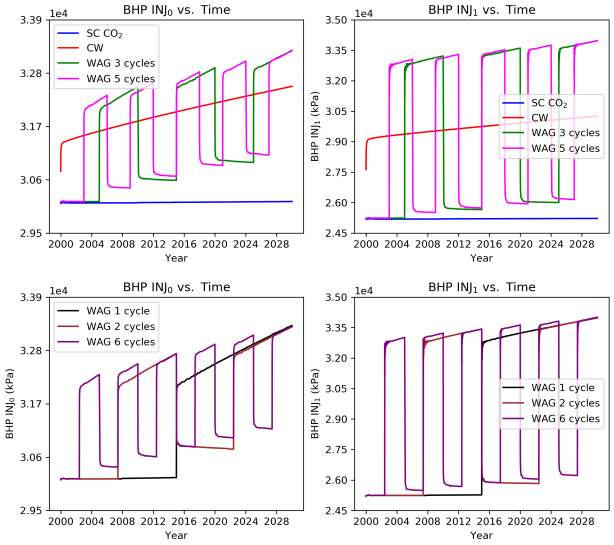

Fig. 15. Bottomhole pressure for the SC-CO_2, CW, and WAG with single and multiple cycles injection cases.

relatively constant. In contrast, when employing Carbonated Water (CW) injection, the higher viscosity of CW, compared to pure SC-CO_2, induces a pronounced pressure surge at the bottomhole, as evident in Fig. 15.

Furthermore, in the cyclic injection scenarios, the pressure remains relatively steady during the injection of pure SC-CO_2, as previously mentioned. However, the subsequent injection of brine, characterized by its incompressibility, triggers a sharp rise in pressure. Additionally, it is noteworthy that due to the deeper location of well INJ0 compared to INJ1, the pressure at the bottom is higher. This pressure variation is illustrated in Fig. 15.

5. Conclusions and recommendations

In this work, different CO_2 trapping mechanisms were studied with a focus on solubility trapping. To achieve this goal, three injection strategies were analyzed: pure supercritical CO_2 (SC-CO_2), carbonated water (CW), and water-alternating-gas (WAG) with 1, 2, 3, 5, and 6 cycles, in which the same amount of CO_2 and brine in term of mass were injected over the whole injection period (30 years) through two horizontal wells. This comprehensive study reveals the effectiveness of these injection strategies and highlights the role of solubility trapping as a prominent and sustainable mechanism for long-term CO_2 geological storage since it is the most effective way to safely store CO_2 underground because it prevents the CO_2 from escaping from the storage formation. Based on the insights gathered from the results, the following conclusions can be inferred:

1) The CW injection strategy is the most favorable among the options, as it enhances sweeping efficiency and CO_2 dissolution, reducing gravity segregation and minimizing residual and structural trapping. This results in safer and more secure geological CO_2 sequestration.
2) The WAG injection strategy shows that increasing cycling frequency enhances solubility trapping compared to pure SC-CO_2 injection. However, as the cycle count rises, the duration of each cycle decreases, eventually resembling continuous CW injection. WAG also reduces CO_2 leakage by breaking the gas into smaller, immobilized blobs and minimizing gravity effects, leading to a more uniform reservoir sweep. Despite its technical advantages, selecting the best injection strategy requires economic analysis, as both CW and WAG involve high water demand, making them costly options.
3) A detailed analysis of the effect of increasing WAG cycles (1-6) on CO_2 trapping mechanisms shows that structural trapping is progressively reduced as more cycles are introduced, while solubility trapping increases. Residual trapping remains significant but is influenced by the rate at which CO_2 is displaced by brine. This suggests that while WAG enhances solubility trapping, an optimal number of cycles must be determined to balance efficiency and operational complexity.
4) While WAG and CW injection strategies offer improved CO_2 sequestration efficiency, their feasibility depends on economic and operational factors. The high water demand for both methods presents a significant challenge, increasing costs and logistical complexity. Further economic feasibility studies are required to assess the trade-offs between improved sequestration efficiency and operational costs.

Conflict of interest

The authors declare no competing interest.

References

Alkan, H., Rivero, F. F., Burachok, O., et al. Engineering design of CO_2 storage in saline aquifers and in depleted

hydrocarbon reservoirs: Similarities and differences. First Break, 2021, 39(6): 69-80.

Agarwal, R. K., Zhang, Z. Optimization of CO_2 sequestration in saline aquifers. Rijeka, Claudia, IntechOpen, 2014.

Ajayi, T., Gomes, J. S., Bera, A. A review of CO_2 storage in geological formations emphasizing modeling, monitoring and capacity estimation approaches. Petroleum Science, 2019, 16: 1028-1063.

Addassi, M., Omar, A., Ghorayeb, K., et al. Comparison of various reactive transport simulators for geological carbon sequestration. International Journal of Greenhouse Gas Control, 2021, 110: 103419.

Alizadeh, A. H., Khishvand, M., Ioannidis, M. A., et al. Multi-scale experimental study of carbonated water injection: An effective process for mobilization and recovery of trapped oil. Fuel, 2014, 132: 219-235.

Burton, M., Bryant, S. L. Eliminating buoyant migration of sequestered CO_2 through surface dissolution: implementation costs and technical challenges. SPE Reservoir Evaluation & Engineering, 2009, 12(3): 399-407.

Bryant, S. L., Lakshminarasimhan, S., Pope, G. A. Buoyancy-dominated multiphase flow and its effect on geological sequestration of CO_2. SPE Journal, 2008, 13(4): 447-454.

Bisweswar, G., Al-Hamairi, A., Jin, S. Carbonated water injection: an efficient EOR approach. A review of fundamentals and prospects. Journal of Petroleum Exploration and Production Technology, 2020, 10: 673-685.

Celia, M. A., Bachu, S., Nordbotten, J. M., et al. Status of CO_2 storage in deep saline aquifers with emphasis on modeling approaches and practical simulations. Water Resources Research, 2015, 51(9): 6846-6892.

Duan, Z., Sun, R., Zhu, C., et al. An improved model for the calculation of CO_2 solubility in aqueous solutions containing Na^+, K^+, Ca^{2+}, Mg^{2+}, Cl^-, and SO_4^{2-}. Marine chemistry, 2006, 98(2-4): 131-139.

Esene, C., Rezaei, N., Aborig, A., et al. Comprehensive review of carbonated water injection for enhanced oil recovery. Fuel, 2019, 237: 1086-1107.

Foroozesh, J., Dier, M. A., Rezk, M. G. A simulation study on CO_2 sequestration in saline aquifers: Trapping mechanisms and risk of CO_2 leakage. MATEC Web Conferences, 2018, 225: 03004.

Foroozesh, J., Jamiolahmady, M. The physics of CO_2 transfer during carbonated water injection into oil reservoirs: From non-equilibrium core-scale physics to field-scale implication. Journal of Petroleum Science and Engineering, 2018, 66: 798-805.

Grobe, M., Pashin, J. C., Dodge, R. L. Carbon dioxide sequestration in geological media-state of the science. Tulsa, USA, American Association of Petroleum Geologists, 2009.

GLOBAL CCS institute. Capturing carbon dioxide (CO_2) is the first step in carbon capture and storage (CCS), a suite of technologies that prevents large quantities of CO_2 from being released into the atmosphere. GLOBAL CCS institute 2023.

Holt, T., Lindeberg, E. Thermal power-without greenhouse gases and with improved oil recovery. Energy Conversion and Management, 1992, 33(5-8): 595-602.

Hassanzadeh, H., Pooladi-Darvish, M., Keith, D. W. Accelerating CO_2 dissolution in saline aquifers for geological storage Mechanistic and sensitivity studies. Energy & Fuels, 2009, 23(6): 3328-3336.

Jikich, S. A., Sams, W. N., Bromhal, G., et al. Carbon dioxide injectivity in brine reservoirs using horizontal wells. In National Energy Technology Laboratory, United States Department of Energy (eds) Proceedings for the 2nd national conference on carbon sequestration, 2003: 5-8.

Leonenko, Y., Keith, D. W. Reservoir engineering to accelerate the dissolution of CO_2 stored in aquifers. Environmental science & technology, 2008, 42(8): 2742-2747.

Miguel, C. V., Mendes, A., Madeira, L. M. An overview of the Portuguese energy sector and perspectives for power-to-gas implementation. Energies, 2018, 11(12): 3259.

Motie, M., Assareh, M. CO_2 sequestration using carbonated water injection in depleted naturally fractured reservoirs: A simulation study. International Journal of Greenhouse Gas Control, 2020, 93: 102893.

Nghiem, L., Shrivastava, V., Kohse, B., et al. Simulation of trapping processes for CO_2 storage in saline aquifers. Paper PETSOC 156 Presented at Canadian International Petroleum Conference, Calgary, Alberta, 16-18 June, 2009.

Orr, L. Carbon capture and sequestration: where do we stand. Global Climate & Energy Project, NAE/AAES Convocation, Washington DC, 19 April, 2010.

Peaceman, D. W. Representation of a horizontal well in numerical reservoir simulation. SPE Advanced Technology Series, 1993, 1(1): 7-16.

Parkhurst, D. L., Appelo, C. A. J. Description of input and examples for PHREEQC version 3-A computer program for speciation, batch-reaction, one-dimensional transport, and inverse geochemical calculations, edited by D. L. Parkhurst and C. A. J. Appelo, U.S. Geological Survey Techniques and Methods, New York, pp. 497, 2013.

Raza, A., Gholami, R., Rezaee, R., et al. Significant aspects of carbon capture and storage-A review. Petroleum, 2019, 5(4): 335-340.

Society of Petroleum Engineers. The 11th Society of Petroleum Engineers Comparative Solution Project: Problem Definition. Society of Petroleum Engineers, 2023.

Sohrabi, M., Riazi, M., Jamiolahmady, M., et al. Carbonated water injection (CWI)-A productive way of using CO_2 for oil recovery and CO_2 storage. Energy Procedia, 2011, 4: 2192-2199.

Sohrabi, M., Riazi, M., Jamiolahmady, M., et al. Carbonated water injection for oil recovery and CO_2 storage. In Sustainable energy UK conference: Meeting the science and engineering challenge, Oxford, UK, 2008.

Sadati, E. Y., Sahraei, E., Rahnema, M., et al. The effect of CO_2-enriched water salinity on enhancing oil recovery and its potential formation damage: an experimental study on shaly sandstone reservoirs. Journal of Petroleum Exploration and Production Technology, 2020, 10: 3791–3802.

Spycher, N., Pruess, K., Ennis-King, J. CO_2-H_2O mixtures in the geological sequestration of CO_2. I. Assessment and calculation of mutual solubilities from 12 to 100 C and up to 600 bar. Geochimica et cosmochimica acta, 2003, 67(16): 3015-3031.

Tariq, Z., Yildirim, E. U., Gudala, M., et al. Spatial-temporal prediction of minerals dissolution and precipitation using deep learning techniques: An implication to Geological Carbon Sequestration. Fuel, 2023, 341: 127677.

Vilarrasa, V., Rutqvist, J. Thermal effects on geologic carbon storage. Earth-science reviews, 2017, 165: 245-256.

Zamani, N., Oldenburg, C. M., Solbakken, J., et al. CO_2 flow modeling in a coupled wellbore and aquifer system: Details of pressure, temperature, and dry-out. International Journal of Greenhouse Gas Control, 2024, 132: 104067.